Dynamic Real-Time Optimization and Control of a Hybrid Energy System

Milana Trifkovic
Dept. of Chemical and Petroleum Engineering, University of Calgary, Calgary, AB, Canada T2N 1N4

W. Alex Marvin and Prodromos Daoutidis
Dept. of Chemical Engineering and Materials Science, University of Minnesota, Minneapolis, MN 55455

Mehdi Sheikhzadeh
Dept. of Instrumentation and Control, Lambton College, Sarnia, ON, Canada N7S 6K4

DOI 10.1002/aic.14458
Published online April 8, 2014 in Wiley Online Library (wileyonlinelibrary.com)

A proactive energy management strategy for a stand-alone hybrid renewable energy system is presented. The study was motivated by the system built in Lambton College (Sarnia, Ontario, Canada) which includes photovoltaic arrays, wind turbine, battery, electrolyzers, hydrogen storage tanks, and fuel cells. The control architecture consists of two levels of hierarchy: (1) optimal predictive scheduling at the supervisory level and (2) local controllers for each of the system units. A "day-ahead" approach is followed at the supervisory level and a bidirectional communication between the supervisory, proactive control, and the low-level control layer is established. The proposed energy management strategy accounts for external (i.e., weather and demand) and internal disturbances. The efficacy of the proposed strategy is demonstrated through case studies. © 2014 American Institute of Chemical Engineers *AIChE J*, 60: 2546–2556, 2014
Keywords: energy, process control, optimization

Introduction

Renewable energy sources (RES) are a key factor toward mitigating carbon emissions due to power generation. The integration of RES into the power infrastructure, although highly desirable from an environmental perspective, is characterized by significant technical challenges.[1]

A key attribute of RES, such as wind and solar resources, is intermittency. RES are not dispatchable, they exhibit large fluctuations, and are uncertain. As a result, only 5% of the total electricity is currently generated from nonhydro RES in the U.S.[2] Strategies for coping with the intermittency of RES for power production exist on both the supply side and the demand side. Supply-side variability can be reduced by combining different RES or through the use of energy storage, whereas programmable loads (e.g., smart appliances) can be used to reduce demand-side variability.[3–7] A supply-side strategy alone has traditionally necessitated the installation of excess RES capacity far above the average power demand, resulting in higher operating costs. To avoid these losses, there has been a growing interest in developing weather forecasting models that would enable more efficient utilization of the generation units.[8,9] A properly designed energy storage stabilizes the system by absorbing and injecting instantaneous power.[10–13] Significant efforts have been invested on demand-side forecasting for building occupancy and design, and power market prices. Such forecasts can allow for the minimization of electricity costs, while maintaining comfortable building conditions.[14–17]

The design of effective hybrid energy systems that involve different RES (e.g., wind and solar) as well as storage devices (hydrogen, compressed air, pumped hydroelectric systems, batteries, and supercapacitors) depends on the location, the operational mode (stand alone vs. grid connected), and their size. Various heuristics,[18–20] as well as simulation-based optimization strategies have been applied to evaluate system designs in different environments.[21–25]

An imperative for operation of any hybrid energy system is the advanced monitorability and control of its assets and operations. Optimization and control algorithms for hybrid energy systems integrate management of the supply side, energy storage and demand side to find the optimal (or near optimal) unit commitment and dispatch of renewable energy so that certain objectives are achieved. A commonly pursued objective for a stand-alone mode of operation is to economically supply a local load, whereas under a grid-connected mode the maximization of profit is typically sought.[26,27] Additional objectives such as the minimization of greenhouse gas emissions by applying heuristic and multiobjective optimization techniques have been reported.[28] Earlier studies have reported power management strategies that are reactive in nature—acting in response to power imbalances between generation and demand.[29–31] Recent research has sought to incorporate predictions to deliver proactive unit commitment. Significant cost savings have been demonstrated when load predictions and weather/ambient condition forecasts are

Correspondence concerning this article should be addressed to M. Trifkovic at mtrifkov@ucalgary.ca.

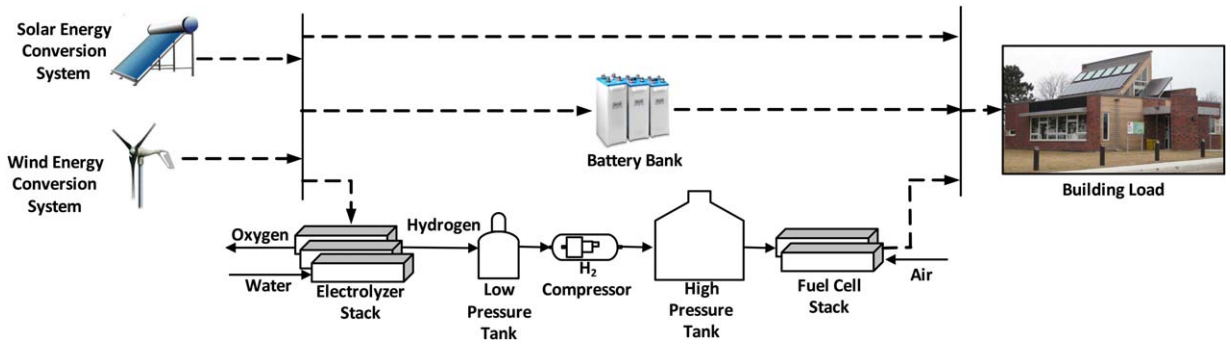

Figure 1. Hybrid energy system structure.

[Color figure can be viewed in the online issue, which is available at wileyonlinelibrary.com.]

included.[32,33] Similarly, grid-connected configurations have been shown to benefit from proactive unit commitment that includes electricity price predictions.[34] The literature on power management studies for different types of hybrid energy systems using optimization is growing rapidly.[35–39] However, only a few of these, either reactive or proactive, algorithms have been implemented in real time due to the high capital cost associated with renewable energy systems.[40,41] Furthermore, the reported case studies are based on simplified models of the different units, especially those related to energy storage.

Our previous work[42,43] was motivated by a hybrid energy system built in Lambton College (Sarnia, Ontario, Canada) which includes photovoltaic arrays, wind turbine, battery, electrolyzers, hydrogen storage tanks, and fuel cells. It developed rigorous process models for each of the system units, a MATLAB-based simulation platform, and a hierarchical control structure which consisted of two layers: supervisory and low-level control. Although the supervisory controller offered fast execution, it was reactive in nature as it addressed only power imbalances between generation and demand. Moreover, the strategy did not have the capability of handling a large-scale hybrid system which may consist of multiple units. In this study, we use the previously developed computational platform (the comprehensive dynamic model and local controllers) and use a dynamic real-time optimization (D-RTO) layer as the supervisory controller. The aim of the new control strategy is to exploit the forecasted disturbance trends in an optimal way, address the system's modular design, and increase the units' lifetime by minimizing the number of startups and shutdowns. As part of the control strategy, we establish a bidirectional communication between the D-RTO and low-level control layer to account for internal as well as exogenous disturbances in the system. Two case studies, demonstrating the effectiveness of the proposed control structure, are presented.

The rest of this article is organized as follows. Sections and present the structure and the control architecture of the hybrid energy system studied. Section lays out the optimization formulation used at the supervisory level. Section discusses the optimization results, and applications of the control structure to the system built in Lambton College. Section concludes this article and presents future research directions.

Hybrid Energy System Structure

The hybrid energy system under study consists of two RES, a local load bus and an energy storage system. The energy storage system is battery and hydrogen based, which increases the flexibility of the hybrid energy system but also its operational complexity. The hybrid energy system structure is shown in Figure 1. The system includes a wind turbine, photovoltaics, three electrolyzers, low- and high-pressure hydrogen tanks, hydrogen compressor, two fuel cells, and a battery subsystem. The generated power from the RES can be used directly to meet the load demand, generate hydrogen (through the electrolyzers), or to charge the battery.

Hydrogen generated by the electrolyzers is stored in the low-pressure hydrogen tank, which then can be used either to run the fuel cells or be compressed and sent to the high-pressure tank. When power generated from the RES is not sufficient to meet the load demand, the power deficit can be corrected by either discharging the battery or activating fuel cells which consume previously stored hydrogen in the low- or high-pressure tank and convert it to electricity. The fuel cell activation occurs only if there is a sufficient supply of hydrogen in the storage tank. Fast, local controllers, which are fully described in Ref. 42, were implemented to assure that each unit operates at its setpoint determined by the supervisory layer. The supervisory layer collects and processes information from the supply, storage and demand-side units about their current and future predicted states and determines the optimal scheduling to assure an uninterrupted satisfaction of energy demand while satisfying the imposed constraints.

Control Architecture

The control architecture is shown in Figure 2. An optimal plan to operate the process units is calculated by the D-RTO layer and sent to the low-level controllers for implementation. The optimal plan consists of the unit commitment (binary controls) and the corresponding power setpoints (continuous controls).

Updated unit states, statuses, and weather and demand forecasts are communicated back to the D-RTO layer periodically. Thus, the control architecture operates in a closed-loop manner. Additionally, the D-RTO layer operates in a moving horizon fashion, with the length of the time horizon desired for the optimal plan remaining constant for each optimization run.

The supervisory controller development was carried out in GAMS while the local controllers and the dynamic model were developed in MATLAB/Simulink. The connection between the two layers was established using the MATLAB/

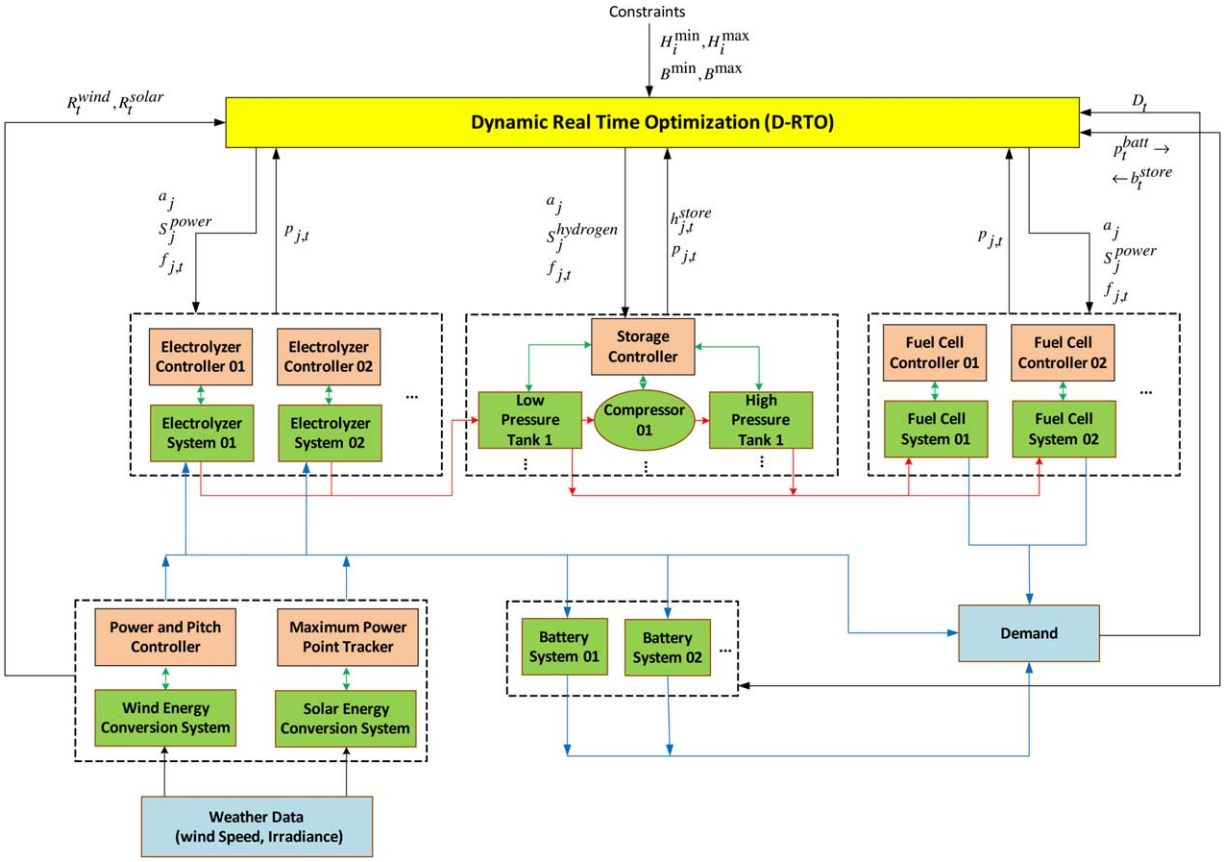

Figure 2. Control architecture.

[Color figure can be viewed in the online issue, which is available at wileyonlinelibrary.com.]

GAMS interface.[44] Interfacing GAMS with MATLAB enabled the use of sophisticated solvers (such as CPLEX) for problems with binary and continuous variables. To reduce the optimization complexity, the supervisory controller uses a time-discretized version of the process model that is simplified to capture only the dynamics relevant in the time scale of the optimization horizon (hours). However, the local controllers for each process unit were simulated using a detailed continuous time nonlinear model. The differing time scales between the supervisory and low-level layer are addressed by a fast dynamic storage system (i.e., battery) which serves to buffer power. Although an approximate battery setpoint is determined by the supervisory layer, it is further refined and adjusted on a smaller sampling interval (1 s) according to the balance between generated and used power. Specifically, the battery charging/discharging is calculated, at the low-level layer, as the difference between power production (i.e., wind, solar, and fuel cells) and power consumption (i.e., electrolyzers, compressor, and power demand). This allows for the rejection of internal disturbances, arising from a malfunction of any of the system units, as well as model mismatch between the supervisory and low-level control layer. Similarly, the low-pressure tank setpoint determined by the supervisory layer can be overwritten in the event that the hydrogen level in the tank is not sufficient to meet the demand. In that case, a remainder is taken from the high-pressure hydrogen tank.

The proposed control strategy addresses the different time scales associated with hybrid energy systems and supports their proactive energy management. It accounts for external and internal disturbances, while minimizing the system communication and the computation time required for the planning.

D-RTO Formulation

The D-RTO layer solves a dynamic optimization problem from the current time t^0 over a time horizon of length t^h. The general problem formulation is

$$\min_{u(\tau)} \int_{t^0}^{t^0+t^h} \varphi(z(\tau), u(\tau), \chi(\tau)) d\tau \tag{1a}$$

$$\text{subject to } \frac{dz}{d\tau} = \mathbf{f}(z(\tau), u(\tau), \chi(\tau)) \tag{1b}$$

$$0 = \mathbf{g}(z(\tau), u(\tau), \chi(\tau)) \tag{1c}$$

$$0 \geq \mathbf{h}(z(\tau), u(\tau), \chi(\tau)) \tag{1d}$$

$$z(t^0) = z^0, \ \forall \tau \in [t^0, t^0 + t^h] \tag{1e}$$

where $z(\tau)$ are the state variables, $u(\tau)$ are the decision variables, and $\chi(\tau)$ are the disturbances. The dynamic model of the system is expressed in (1b,c) with operating constraints in (1d), and initial states in (1e).

By discretizing the time horizon into time periods $t \in \{1, \ldots, T\}$ with uniform duration $\Delta t = t^h/T$, the general dynamic program (1) can be reformulated as

$$\min_{u(t)} \ \Delta t \cdot \sum_t \varphi(z(t), u(t), \chi(t)) \tag{2a}$$

$$\text{subject to } z(t) = \Delta t \cdot \mathbf{f}(z(t), u(t), \chi(t)) + z(t-1) \tag{2b}$$

$$0=\mathbf{g}(z(t),u(t),\chi(t)) \tag{2c}$$

$$0\geq\mathbf{h}(z(t),u(t),\chi(t)) \tag{2d}$$

$$z(0)=z^0,\ \forall t\in\{1,\ldots,T\} \tag{2e}$$

which is a linear or nonlinear program, depending on the functional form of **f**, **g**, and **h**.

Dynamic model

For the specific hybrid energy system considered, the dynamic model (2b,c) arises from mass and energy conservation equations. State variables are the storage levels for hydrogen in tanks and energy in batteries. Decision variables are the RES utilization (wind and solar), power and hydrogen usage/generation for each process unit, and the unit commitments. Disturbances are the wind and solar availability, and power demand. The dynamic model is linear with respect to the state variables, decision variables, and disturbances. As the operating constraints are also linear and some of the decision variables (i.e., unit commitments) are binary, our D-RTO is a mixed integer linear program. The specific objective function and constraints are discussed in the following subsections.

Subscripts and sets are used to distinguish process units and tanks. A process unit j is in the set $\mathbf{J}$, which includes water electrolyzers $\mathbf{J}^e\subset\mathbf{J}$, hydrogen fuel cells $\mathbf{J}^f\subset\mathbf{J}$, and gas compressors $\mathbf{J}^c\subset\mathbf{J}$. A tank for hydrogen storage i is in the set $\mathbf{I}$, which includes low-pressure $\mathbf{I}^l\subset\mathbf{I}$ and high-pressure $\mathbf{I}^h\subset\mathbf{I}$ subsets.

Objective function

Multiple objective functions may be of interest for the D-RTO of hybrid energy systems. We choose to maximize the utilization of renewable resources (u_t^{wind} and u_t^{solar}) and amount of stored hydrogen ($h_{i,t}^{\text{store}}$), and to minimize the number of system unit startups ($y_{j,t}$). Scalarization of these objectives forms the single objective of the D-RTO

$$\max\sum_{i,j,t}\left(C^w u_t^{\text{wind}}+C^s u_t^{\text{solar}}+C^h h_{i,t}^{\text{store}}-C^y y_{j,t}\right) \tag{3}$$

where C^w, C^s, C^h, C^y are the corresponding weight factors. The weight factors were chosen based on the electricity cost equivalent to the power produced from renewable energy, hydrogen cost, and depreciation cost of fuel cell associated with each startup. The cost of electricity was assumed to be 10 ¢/kWh, the cost of hydrogen (99.9% purity) was provided by the local distributor and estimated to be \$33.7/m^3, and the startup cost for the fuel cell was approximated to be \$0.46/cycle based on the manufacturer's data for the maximum number of on-off cycles for the fuel cell used in the system.

Constraints

Power demand D_t is satisfied in each time period through a balance of utilized wind u_t^{wind} and solar u_t^{solar} resources, net power generation $p_{j,t}$ of process units (electrolyzers, fuel cells, and compressors), and battery charging/dischanging p_t^{batt}

$$u_t^{\text{wind}}+u_t^{\text{solar}}+\sum_j p_{j,t}-p_t^{\text{batt}}=D_t,\ \forall t \tag{4}$$

Utilized wind and solar resources cannot exceed the amounts harvestable

$$u_t^{\text{wind}}\leq R_t^{\text{wind}},\ \forall t \tag{5}$$

$$u_t^{\text{solar}}\leq R_t^{\text{solar}},\ \forall t \tag{6}$$

Each unit can be on for some fraction $f_{j,t}$ of each time period. If unit j is on at any point during t, then the binary variable $a_{j,t}$ is true

$$f_j^{\min}\cdot a_{j,t}\leq f_{j,t}\leq a_{j,t},\ \forall j,t \tag{7}$$

$$0\leq f_{j,t}\leq 1,\ \forall j,t \tag{8}$$

$$a_{j,t}\in\{0,1\},\ \forall j,t \tag{9}$$

where $f_j^{\min}$ is the minimum time that unit j can be operated.

It would be inefficient to run any electrolyzer while a fuel cell is operational, and vice versa. This is enforced by

$$a_{j,t}+a_{j',t}\leq 1,\ \forall t, j\in\mathbf{J}^e, j'\in\mathbf{J}^f \tag{10}$$

The binary variable $y_{j,t}$ is true if unit j turns from off to on during time period t. This is accomplished with the constraints

$$y_{j,t}\geq a_{j,t}-a_{j,t-1},\ \forall j,t \tag{11}$$

$$y_{j,t}\leq a_{j,t},\ \forall j,t \tag{12}$$

$$a_{j,0}=a_j^0,\ \forall j \tag{13}$$

where a_j^0 is the initial state of each unit.

If a unit was operating in the previous time period and operates in the next time period, two scenarios can occur for the present time period. Either the unit is shut down briefly (i.e., $f_{j,t}<1$, $y_{j,t}=1$) or the unit operates for the whole time period (i.e., $f_{j,t}=1$, $y_{j,t}=0$). This is enforced by

$$f_{j,t}\geq a_{j,t-1}+a_{j,t}+a_{j,t+1}-2-y_{j,t},\ \forall j,t \tag{14}$$

Once turned on, the process unit quickly reaches the power setpoint S_j^{power} and hydrogen setpoint S_j^{hydrogen}. Note that these setpoints are negative, positive, or zero for consumers, generators, and uninvolved process units, respectively. The amount of generated/consumed power and hydrogen during the time period is then

$$p_{j,t}=S_j^{\text{power}}\cdot f_{j,t},\ \forall j,t \tag{15}$$

$$h_{j,t}=S_j^{\text{hydrogen}}\cdot f_{j,t},\ \forall j,t \tag{16}$$

Hydrogen produced by the electrolyzers is sent to low-pressure tanks. Low-pressure hydrogen can then be compressed and sent to high-pressure tanks or sent to fuel cells. Hydrogen in high-pressure tanks can also be sent to fuel cells. These are captured by the following relations

$$h_{j,t}=\sum_{i\in\mathbf{I}^l}h_{i,j,t}^{\text{gen}},\ \forall j\in\mathbf{J}^e,t \tag{17}$$

$$h_{i,t}^{\text{store}}=h_{i,t-1}^{\text{store}}+\sum_{j\in\mathbf{J}^e}h_{i,j,t}^{\text{gen}}-\sum_{i'\in\mathbf{I}^h,j\in\mathbf{J}^c}h_{i,i',j,t}^{\text{comp}}-\sum_{j\in\mathbf{J}^f}h_{i,j,t}^{\text{cons}},\ \forall i\in\mathbf{I}^l,t \tag{18}$$

$$h_{j,t}=\sum_{i\in\mathbf{I}^l,i'\in\mathbf{I}^h}h_{i,i',j,t}^{\text{comp}},\ \forall j\in\mathbf{J}^c,t \tag{19}$$

$$h_{i,t}^{\text{store}}=h_{i,t-1}^{\text{store}}+\sum_{i\in\mathbf{I}^l,j\in\mathbf{J}^c}h_{i,i',j,t}^{\text{comp}}-\sum_{j\in\mathbf{J}^f}h_{i,j,t}^{\text{cons}},\ \forall i\in\mathbf{I}^h,t \tag{20}$$

$$h_{j,t}=\sum_i h_{i,j,t}^{\text{cons}},\ \forall j\in\mathbf{J}^f,t \tag{21}$$

Table 1. Hybrid Energy System Design

Unit Name	Rating Power (kW)	Number of Units
Wind system	8	1
Solar system	2.2	1
Electrolyzer 1	2.3	1
Electrolyzer 2	1.1	2
Fuel cell	1.1	2
Compressor	2.3	1
Battery	2	1

Power can be stored or discharged from the battery as needed

$$b_t^{\text{store}} = b_{t-1}^{\text{store}} + p_t^{\text{batt}}, \ \forall t \tag{22}$$

Hydrogen storage and battery storage are bounded and have specified initial conditions

$$H_i^{\min} \le h_{i,t}^{\text{store}} \le H_i^{\max}, \ \forall i,t \tag{23}$$

$$B^{\min} \le b_t^{\text{store}} \le B^{\max}, \ \forall t \tag{24}$$

$$h_{i,0}^{\text{store}} = H_i^0, \ \forall i \tag{25}$$

$$b_0^{\text{store}} = B^0 \tag{26}$$

Simulation Results

The hybrid system units and their corresponding power ratings are summarized in Table 1. The details of the design of the system can be found elsewhere.[42] The presented simulation results are based on average weather data (wind velocity and solar irradiance) for a 24-hour period in the month of June in the Sarnia, Ontario region, and a typical load demand of the hybrid system (see Figure 3).

The D-RTO calculates a "day-ahead" optimal plan using an optimization horizon t^h of 24 h with 1-hour time periods ($\Delta t = 1$ h). Bidirectional communication between the D-RTO and low-level controllers occurs every 1 h. At these times, the low-level control layer sends the current and forecasted demand (D_t) and the RES power profiles (R_t^{wind} and R_t^{solar}), as well as the amount of stored hydrogen in tanks (H_i^0), battery charge status (B^0) and the unit status (a_j^0). The D-RTO layer returns the unit commitment for the electrolyzers, fuel cells and compressor ($a_{j,t}$), the fraction of the time period that units were on ($f_{j,t}$), the unit power setpoints ($p_{j,t}$), the battery charge and discharge power (p_t^{batt}), as well as the output hydrogen flow rates from the low- and high-pressure hydrogen tanks ($h_{i,j,t}^{\text{cons}}$). Note that the hierarchical scheme introduced in this article relies on credible forecasts. Without this assumption, the proactive actions cannot be guaranteed to be effective and the system performance would degrade. The CPU time for to solve each 1-hour simulation in MATLAB was approximately 30 s, while the calculation of a "day-ahead" optimal plan in GAMS was obtained in less than 1 s.

Table 2 presents the proportional-integral-derivative (PID) and model predictive control (MPC) tuning parameters for the low-level controller applied on the wind turbine, fuel cell and electrolyzer subsystems.[42] In this table, k_c, τ_i, τ_d, are the proportional, integral, and derivative constants, and $W_y = 15$, $W_u = 8$ are the prediction and control horizon, respectively.

To illustrate the proactiveness and robustness of the control strategy, we present the optimal setpoint trajectories for the selected units after the first, fifth, and tenth optimization interval ($\text{Opt}_{1,5,10}$) in Figure 4. The initial plan based on the daily optimization (shown by the dashed lines) was altered in the future optimization intervals as a result of the feedback from the low-level control layer. The updated states were used as initial conditions for the calculation of the next optimal trajectory, and the future weather and demand trends were revised, which consequently altered the optimal plan for the next 24 h. The Opt_{10} scenario (shown by the solid lines) started with Electrolyzer 1 at its rated power. This indicates that the unit was on in the previous interval (Opt_9), and its previous state was used as the initial condition in the current (Opt_{10}) optimization interval.

The realized power trajectories for each unit (after 24 optimization intervals) are shown in Figure 5. The figure inset shows the time it takes for the electrolyzer to reach the setpoint determined by the D-RTO level and depicts the model dynamics as well as the control action at the

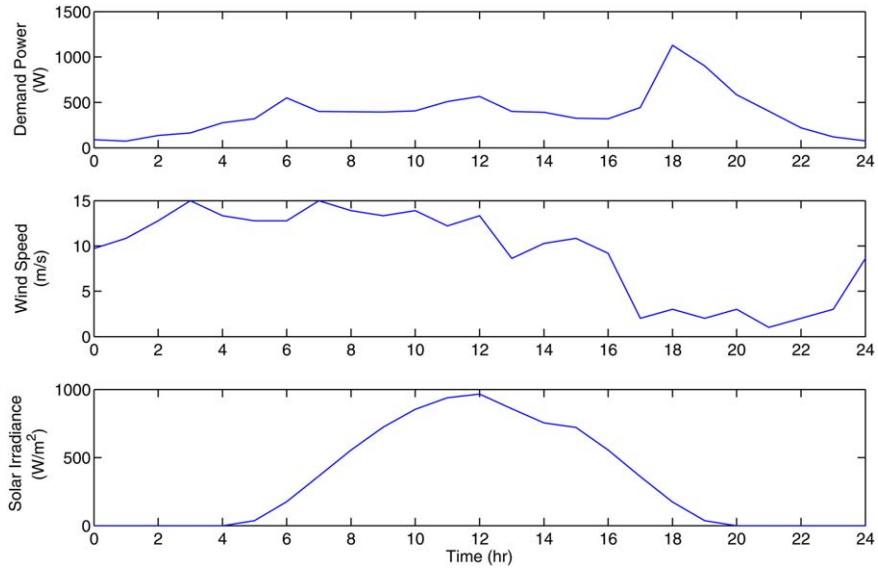

Figure 3. Demand, wind velocity, and solar irradiance data for 24 h.

[Color figure can be viewed in the online issue, which is available at wileyonlinelibrary.com.]

Table 2. Controller Tuning Parameters

Unit	Controller	Tuning Parameters
Wind turbine pitch	Reference pitch	PD controller: $k_c = 35$, $\tau_d = 0.2$
	Pitch angle	P controller: $k_c = 500$
Wind turbine power	Rotor side current	PI controller: $k_c = 0.3$, $\tau_i = 0.037$
	Grid side current	PI controller: $k_c = 1$, $\tau_i = 0.01$
	Voltage	PI controller: $k_c = 0.02$, $\tau_i = 0.4$
Fuel cell	Hydrogen flow	PI controller: $k_c = 1.2$, $\tau_i = 0.01$
	Air humidity	P controller: $k_c = 1$
	Fuel cell power	MPC controller: $W_y = 10$, $W_u = 4$
Electrolyzer	Electrolyzer power	MPC controller: $W_y = 15$, $W_u = 8$

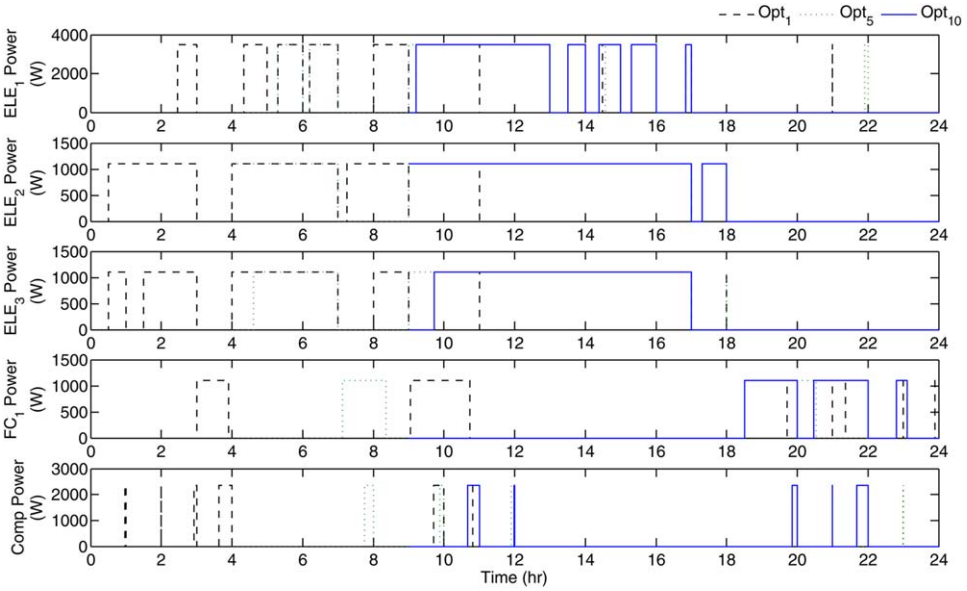

Figure 4. Estimated power setpoint for each subsystem calculated by D-RTO at $t = 0$ h (Opt_1), $t = 4$ h (Opt_5), and $t = 9$ h (Opt_{10}).

[Color figure can be viewed in the online issue, which is available at wileyonlinelibrary.com.]

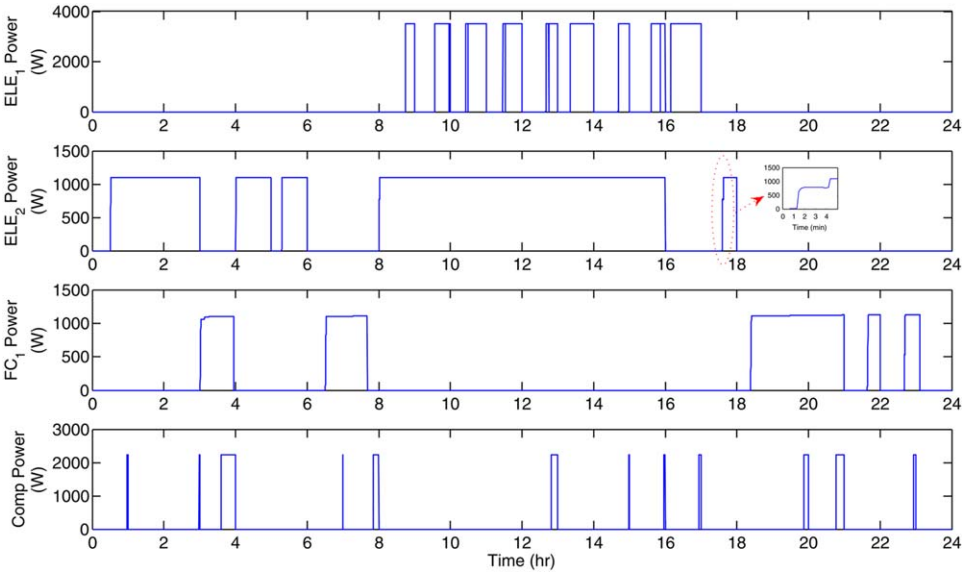

Figure 5. Realized power for hybrid energy system components.

[Color figure can be viewed in the online issue, which is available at wileyonlinelibrary.com.]

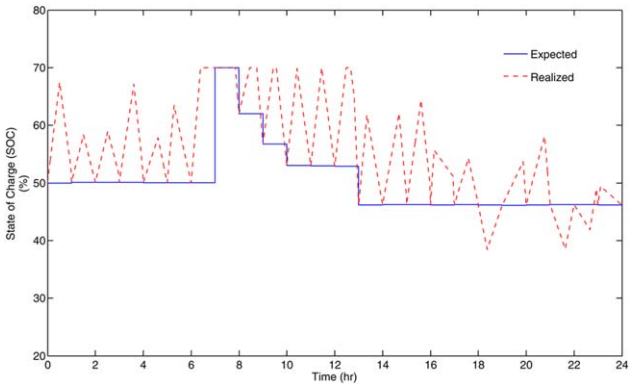

Figure 6. Expected and realized battery SOC.

[Color figure can be viewed in the online issue, which is available at wileyonlinelibrary.com.]

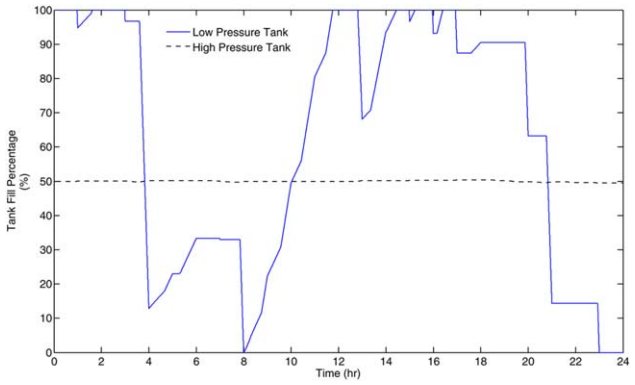

Figure 7. Low- and high-pressure hydrogen tank fill percentage.

[Color figure can be viewed in the online issue, which is available at wileyonlinelibrary.com.]

low-level control layer. Although the majority of the predicted unit commitments were realized, the length of the intervals and the units were utilized differed. Due to the high availability of the RES during this period, all the electrolyzers and the compressor are utilized frequently, while only one of the fuel cells is activated when the demand exceeds the power generated from the RES.

Figure 6 shows the battery dynamics and its variation from the setpoints determined by the D-RTO layer. As mentioned previously, the battery serves as a buffer at the low-level control layer. The realized battery state of charge (SOC) followed the overall trend determined by the D-RTO, but it differs from it within the 1-hour optimization interval, as the low-level layer adjusts the setpoint on a smaller sampling interval (1 s).

The low- and high-pressure hydrogen tanks act as a short-term and long-term hydrogen storage, respectively. The fill percentage for each tank is presented in Figure 7. From the depicted profiles, it can be seen that the low-pressure tank served as the main supply of hydrogen for the fuel cells due to the high RES availability during this period. Also, when it approached its maximum capacity, its content was sent to the compressor and subsequently to the high-pressure tank. Hydrogen from the high-pressure tank was used when the available RES was insufficient to meet the demand, and consequently the fuel cell was activated. The output flow rates ($h_{i,j,t}^{\text{cons}}$) from each tank were estimated by the D-RTO algorithm. The high-pressure hydrogen tank was utilized only when the low-pressure tank was not sufficient to meet hydrogen demand, as there was a cost associated with storing hydrogen in the high-pressure tank (the compressor had to be activated and power used). Note that the compressor and the high-pressure tank in this system are purposely oversized, as the strategic plan of Lambton College is to expand the hybrid energy system and use generated hydrogen for other purposes as well. Consequently, a large amount of power was needed to run the compressor, which was the main reason for the short time intervals that the compressor was activated.

The flow rates from the low-and high-pressure hydrogen tanks could be overwritten at the low-level control layer in the event that the pressure in the tank is not sufficient to meet the fuel cells' demand. The low-level flow controller receives the D-RTO's flow rate setpoints as well as the updated tank content on a one-second basis. If the amount of hydrogen in the tanks is sufficient to meet the fuel cells' demand, the calculated flow rates are enforced. Otherwise, the flow rate controller rejects the D-RTO decision and determines the flow rates according to the tanks' current status. A priority is still given to the low-pressure tank, with any remainder fulfilled with hydrogen from the high-pressure tank. This change in the tank storage level is communicated to the D-RTO layer in the next optimization interval.

Figure 8 depicts the realized power trends of all the system units, and illustrates the overall performance of the hybrid energy system. Each component except the battery (which serves as a power buffer) is shown by the stacked area. The power generators are stacked above and power users below zero. The difference between the two should equate to the battery's power (shown by the solid line). The graph shows that the RES were utilized efficiently through either meeting the demand or storing hydrogen. The battery's dynamic also illustrates that it successfully provided the power balance between the power generators and power users in the system.

To further assess the effectiveness of the proposed control strategy, simulations were performed for 1-year period using again an hourly optimization interval. The load demand, weather data, along with the demand satisfaction and RES utilization are shown in Figure 9. As it can be seen, the demand is satisfied at all times, whereas RES are not utilized only at few instances during the summer. Figure 10 shows the low- and high-pressure tank fill percentage. The yearly trend is similar to that of 24 h one, the low-pressure tank is utilized more frequently and serves as the main hydrogen supply. It can be also seen that at the end of the summer, after the period of continuously high irradiance levels, the high-pressure tank was filled completely. During this period, instances of underutilized RES occurred (Figure 9). However, during the fall and winter, hydrogen stored in the high-pressure tank was effectively used to supplement the shortage in RES. The end-of-year balance in the high-pressure tank was higher by 10% in comparison to the beginning of the year. Considering that year-to-year RES levels and demand can vary, the simulation results show that the design, as well as power management strategy, was suitable for this system. The excess hydrogen could be also sold to improve the economics of the system.

Figure 11 depicts the realized power for hybrid energy system components. The most frequently utilized units were the first electrolyzer (the largest one) and the first of the two fuel cells. The other two electrolyzers were utilized more during the summer when excess of solar energy is present.

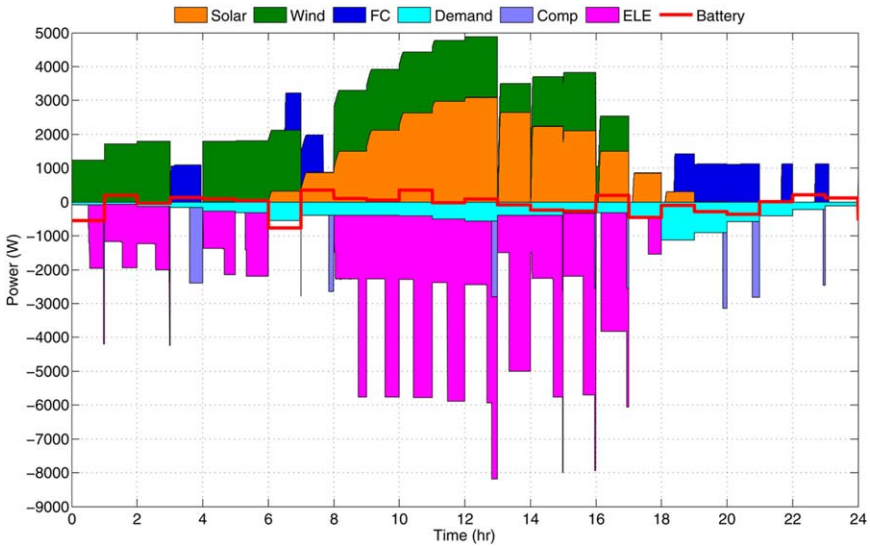

Figure 8. Power balance of the hybrid energy system.

[Color figure can be viewed in the online issue, which is available at wileyonlinelibrary.com.]

One fuel cell was mainly sufficient to satisfy the demand, whereas the second fuel cell was utilized in instances when renewable energy was not available and the demand was higher than the capacity of the first fuel cell. The compressor was utilized frequently to compress hydrogen from the low-pressure tank into the high-pressure tank.

Conclusions

The concept of a hybrid energy system, which corresponds to the coordinated operation of load, renewable power generators, and energy storage systems, is quite appealing due to its flexibility, controllability, and energy management capabilities. To provide uninterrupted power supply, such a system has to economically meet the demand on an instantaneous basis. This article has proposed a proactive hierarchical energy management strategy for the hybrid energy system built in Lambton College, Sarnia, Canada. Although the study was motivated by this particular system, the proposed control strategy is applicable for optimal operation of buildings capable of accommodating multiple units in standalone operation. The proposed strategy consists of long-term resource scheduling by the D-RTO supervisory layer and fast response to any unforeseen internal or external

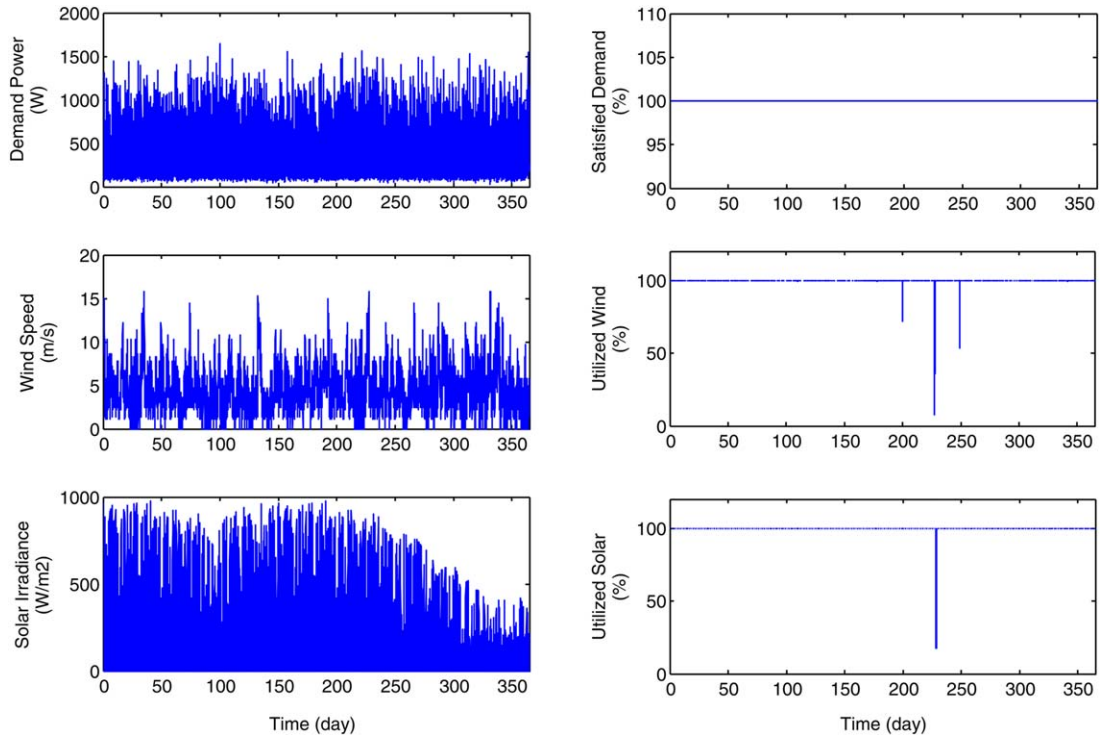

Figure 9. Yearly data for demand, wind velocity, solar irradiance, demand satisfaction, wind and PV utilization.

[Color figure can be viewed in the online issue, which is available at wileyonlinelibrary.com.]

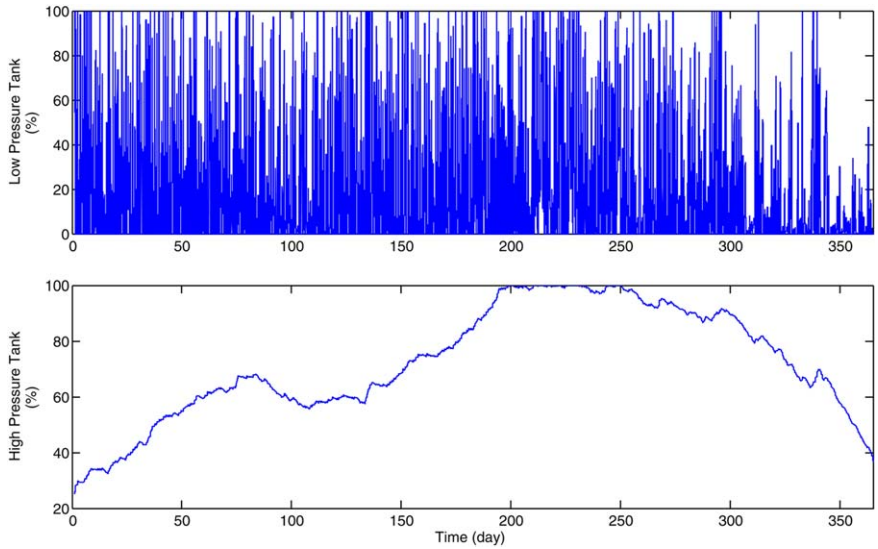

Figure 10. Yearly data for low- and high-pressure hydrogen tank fill percentage.

[Color figure can be viewed in the online issue, which is available at wileyonlinelibrary.com.]

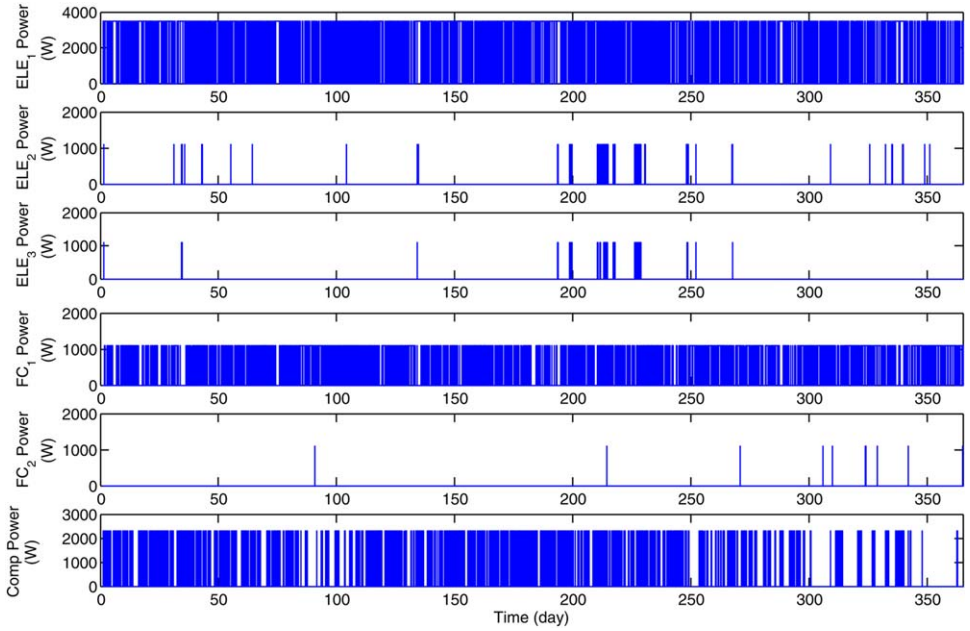

Figure 11. Realized power for hybrid energy system components for 1 year.

[Color figure can be viewed in the online issue, which is available at wileyonlinelibrary.com.]

disturbance (demand or supply). The supervisor utilizes a discrete time model formulation with 1-hour time periods, but maintains good time resolution by allowing for process unit activity for a fraction of a time period. The feedback from the low-level to the D-RTO control layer allowed for incorporation of changes in the system states as well as any internal disturbances arising from a malfunction of system units. At the low-level control layer, the fast energy storage served to buffer power and respond to the fast dynamic changes in the system. The performance of the control strategy was demonstrated through a case study with hydrogen and battery as storage systems. The D-RTO layer added a proactive feature to the overall control architecture with a high level of flexibility to integrate various operational, economical, and safety objectives. Future work will involve implementation of the control strategy presented here along with the previously developed one (reactive in nature) in real time, and will quantify the benefits of the proactive energy management.

Acknowledgments

The authors would like to thank BlueWater Power Inc. for the financial support and valuable suggestions, as well as the Renewable Energy Conversion and Storage Research (RECSR) team at Lambton College. Partial financial support from IREE Project RL-0010-13 is also gratefully acknowledged.

Notation

Sets, subsets, and indexes

$i \in \mathbf{I}$ = tanks for hydrogen storage
$\mathbf{I}^l \subset \mathbf{I}$ = low-pressure tanks
$\mathbf{I}^h \subset \mathbf{I}$ = high-pressure tanks
$j \in \mathbf{J}$ = process units
$\mathbf{J}^e \subset \mathbf{J}$ = water electrolyzers
$\mathbf{J}^f \subset \mathbf{J}$ = hydrogen fuel cells
$\mathbf{J}^c \subset \mathbf{J}$ = gas compressors
$t \in \{1, \ldots, T\}$ = time periods used for optimization.

Parameters

T = number of time periods for optimization
t^0 = current time, s
t^h = length of time horizon, s
Δt = length of each time period for optimization, s
C^w = weight factor associated with maximizing wind utilization
C^s = weight factor associated with maximizing solar utilization
C^h = weight factor associated with maximizing stored hydrogen
C^y = weight factor associated with minimizing unit startups
D_t = power demand during t, W
R_t^{wind} = amount of harvestable wind power during t, W
R_t^{solar} = amount of harvestable solar power during t, W
$f_j^{\min}$ = minimum fraction of a time period that unit j can be operated
S_j^{power} = power setpoint for unit j, W
S_j^{hydrogen} = hydrogen generation setpoint for unit j, mol per Δt
$H_i^{\min}$ = minimum hydrogen storage amount for tank i, mol
$H_i^{\max}$ = maximum hydrogen storage amount for tank i, mol
H_j^0 = initial amount of hydrogen storage in tank i, mol
$B^{\min}$ = minimum battery storage level, W
$B^{\max}$ = maximum battery storage level, W
B^0 = initial battery storage level, W
a_j^0 = initial state (binary) of unit j

Decision variables

u_t^{wind} = amount of harvested wind power during t, W
u_t^{solar} = amount of harvested solar power during t, W
$p_{j,t}$ = net power generation of unit j during t, W
p_t^{batt} = battery charging during t, W
b_t^{store} = power stored in battery at the end of t, W
$h_{i,t}^{\text{store}}$ = amount of hydrogen stored in tank i at the end of t, mol
$h_{j,t}$ = amount of hydrogen generated by unit j during t, mol
$h_{i,j,t}^{\text{gen}}$ = amount of hydrogen sent from electrolyzer $j \in \mathbf{J}^e$ to low-pressure tank $i \in \mathbf{I}^l$ during t, mol
$h_{i,i',j,t}^{\text{comp}}$ = amount of hydrogen sent from low-pressure tank $i \in \mathbf{I}^l$ to high-pressure tank $i' \in \mathbf{I}^h$ using compressor $j \in \mathbf{J}^c$ during t, mol
$h_{i,j,t}^{\text{cons}}$ = amount of hydrogen sent from tank i to fuel cell $j \in \mathbf{J}^f$ during t, mol
$f_{j,t}$ = fraction of time period t that unit j is on
$a_{j,t}$ = binary variable equal to 1 if unit j is on at any point during t
$y_{j,t}$ = binary variable equal to 1 if unit j starts up during t.

Literature Cited

1. Giannakis GB, Kekatos V, Gatsis N, Kim S-J, Zhu H, Wollenberg BF. Monitoring and optimization for power grids: a signal processing perspective. *IEEE Signal Process Mag.* 2013;30(5):107–128. arXiv:1302.0885.
2. *Annual Energy Outlook 2013, Technical Report*. U.S. Energy Information Administration, 2013.
3. Karki R, Billinton R. Reliability/cost implications of PV and wind energy utilization in small isolated power systems. *IEEE Trans Energy Conversion.* 2001;16(4):368–373. doi:10.1109/60.969477.
4. Santarelli M, Cal M, Macagno S. Design and analysis of stand-alone hydrogen energy systems with different renewable sources. *Int J Hydrogen Energy.* 2004;29(15):1571–1586. doi:10.1016/j.ijhydene.2004.01.014.
5. Yang H, Lu L, Zhou W. A novel optimization sizing model for hybrid solar-wind power generation system. *Solar Energy.* 2007;81(1):76–84. doi:10.1016/j.solener.2006.06.010.
6. Giannakoudis G, Papadopoulos AI, Seferlis P, Voutetakis S. Optimum design and operation under uncertainty of power systems using renewable energy sources and hydrogen storage. *Int J Hydrogen Energy.* 2010;35(3):872–891. doi:10.1016/j.ijhydene.2009.11.044.
7. Powell KM, Edgar TF. Modeling and control of a solar thermal power plant with thermal energy storage. *Chem Eng Sci.* 2012;71:138–145. doi:10.1016/j.ces.2011.12.009.
8. Botterud A, Zhou Z, Wang J, Bessa RJ, Keko H, Sumaili J, Miranda V. Wind power forecasting, unit commitment, and electricity market operations, In: 2011 IEEE Power and Energy Society General Meeting, Detroit, MI, 2011:1–2. doi:10.1109/PES.2011.6039192.
9. Pappala V, Erlich I, Rohrig K, Dobschinski J. A stochastic model for the optimal operation of a wind-thermal power system. *IEEE Trans Power Syst.* 2009;24(2):940–950. doi:10.1109/TPWRS.2009.2016504.
10. Abbey C, Joos G. Supercapacitor energy storage for wind energy applications. *IEEE Trans Ind Appl.* 2007;43(3):769–776. doi:10.1109/TIA.2007.895768.
11. Teleke S, Baran M, Huang A, Bhattacharya S, Anderson L. Control strategies for battery energy storage for wind farm dispatching. *IEEE Trans Energy Conversion.* 2009;24(3):725–732. doi:10.1109/TEC.2009.2016000.
12. Mercier P, Cherkaoui R, Oudalov A. Optimizing a battery energy storage system for frequency control application in an isolated power system. *IEEE Trans Power Syst.* 2009;24(3):1469–1477. doi:10.1109/TPWRS.2009.2022997.
13. Thounthong P, Rael S, Davat B. Analysis of supercapacitor as second source based on fuel cell power generation. *IEEE Trans Energy Conversion.* 2009;24(1):247–255. doi:10.1109/TEC.2008.2003216.
14. Exarchakos L, Leach M, Exarchakos G. Modelling electricity storage systems management under the influence of demand-side management programmes. *Int J Energy Res.* 2009;33(1):62–76. doi:10.1002/er.1473.
15. Rios-Zalapa R, Wang X, Wan J, Cheung K. Robust dispatch to manage uncertainty in real time electricity markets. In: *2010 Innovative Smart Grid Technologies (ISGT)*, Gaithersburg, MD, 2010:1–5. doi:10.1109/ISGT.2010.5434761.
16. Guan X, Xu Z, Jia Q-S. Energy-efficient buildings facilitated by microgrid. *IEEE Trans Smart Grid.* 2010;1(3):243–252. doi:10.1109/TSG.2010.2083705.
17. Gatsis N, Giannakis GB. Residential load control: distributed scheduling and convergence with lost AMI messages. *IEEE Trans Smart Grid.* 2012;3(2):770–786. doi:10.1109/TSG.2011.2176518.
18. Senjyu T, Hayashi D, Yona A, Urasaki N, Funabashi T. Optimal configuration of power generating systems in isolated island with renewable energy. *Renewable Energy.* 2007;32(11):1917–1933. doi:10.1016/j.renene.2006.09.003.
19. Katsigiannis YA, Georgilakis PS. Optimal sizing of small isolated hybrid power systems using tabu search. *J Optoelectron Adv Mater.* 2008;10(5):1241–1245.
20. Ekren O, Ekren BY. Size optimization of a PV/wind hybrid energy conversion system with battery storage using simulated annealing. *Appl Energy.* 2010;87(2):592–598. doi:10.1016/j.apenergy.2009.05.022.
21. Ter-Gazarian A, Kagan N. Design model for electrical distribution systems considering renewable, conventional and energy storage units. In: *IEE Proceedings C (Generation, Transmission and Distribution)*, Vol. 139, 1992:499–504. doi:10.1049/ip-c.1992.0069.
22. Vallem MR, Mitra J. Siting and sizing of distributed generation for optimal microgrid architecture. In: *Proceedings of the 37th Annual North American Power Symposium*, Ames, IA, 2005:611–616. doi:10.1109/NAPS.2005.1560597.
23. Garcia RS, Weisser D. A wind–diesel system with hydrogen storage: Joint optimisation of design and dispatch. *Renewable Energy.* 2006;31(14):2296–2320. doi:10.1016/j.renene.2005.11.003.
24. Bernal-Agustín JL, Dufo-López R. Simulation and optimization of stand-alone hybrid renewable energy systems. *Renewable Sustainable Energy Rev.* 2009;13(8):2111–2118. doi:10.1016/j.rser.2009.01.010.
25. Tan CW, Green TC, Hernandez-Aramburo CA. A stochastic method for battery sizing with uninterruptible-power and demand shift capabilities in pv (photovoltaic) systems. *Energy.* 2010;35(12):5082–5092. doi:10.1016/j.energy.2010.08.007.
26. Alvarez E, Lopez AC, Gomez-Aleixandre J, de Abajo N. On-line minimization of running costs, greenhouse gas emissions and the impact of distributed generation using microgrids on the electrical system. In: *2009 IEEE PES/IAS Conference on Sustainable*

Alternative Energy (SAE), Valencia, Spain, 2009:1–10. doi:10.1109/SAE.2009.5534847.
27. Stluka P, Godbole D, Samad T. Energy management for buildings and microgrids. In: *50th IEEE Conference on Decision and Control and European Control Conference*, Orlando, FL, 2011:5150–5157. doi:10.1109/CDC.2011.6161051.
28. Colson CM, Nehrir MH, Pourmousavi SA. Towards real-time microgrid power management using computational intelligence methods. In: I*EEE PES General Meeting*, Minneapolis, MN, 2010:1–8. doi:10.1109/PES.2010. 5588053.
29. Valenciaga F, Puleston P. Supervisor control for a stand-alone hybrid generation system using wind and photovoltaic energy. *IEEE Trans Energy Conversion.* 2005;20(2):398–405. doi:10.1109/TEC.2005.845524.
30. Wang C, Nehrir MH. Power management of a stand-alone wind/photovoltaic/fuel cell energy system. *IEEE Trans Energy Conversion.* 2008;23(3):957–967. doi:10.1109/TEC.2007.914200.
31. Ipsakis D, Voutetakis S, Seferlis P, Stergiopoulos F, Elmasides C. Power management strategies for a stand-alone power system using renewable energy sources and hydrogen storage. *Int J Hydrogen Energy.* 2009;34(16):7081–7095. doi:10.1016/j.ijhydene.2008.06.051.
32. Zavala VM, Constantinescu EM, Krause T, Anitescu M. On-line economic optimization of energy systems using weather forecast information. *J Process Control.* 2009;19(10):1725–1736. doi:10.1016/j.jprocont.2009.07.004.
33. Constantinescu EM, Zavala VM, Rocklin M, Lee S, Anitescu M. A computational framework for uncertainty quantification and stochastic optimization in unit commitment with wind power generation. *IEEE Trans Power Syst.* 2011;26(1):431–441. doi:10.1109/TPWRS.2010.2048133.
34. Qi W, Liu J, Chen X, Christofides PD. Supervisory predictive control of standalone wind/solar energy generation systems. *IEEE Trans Control Syst Technol.* 2011;19(1):199–207. doi:10.1109/TCST.2010.2041930.
35. Choi M-E, Kim S-W, Seo S-W. Energy management optimization in a battery/supercapacitor hybrid energy storage system. *IEEE Trans Smart Grid.* 2012;3(1):463–472. doi:10.1109/TSG.2011.2164816.
36. De Brabandere K, Bolsens B, Van den Keybus J, Woyte A, Driesen J, Belmans R. A voltage and frequency droop control method for parallel inverters. *IEEE Trans Power Electron.* 2007;22(4):1107–1115. doi:10.1109/TPEL.2007.900456.
37. Marnay C, Venkataramanan G, Stadler M, Siddiqui A, Firestone R, Chandran B. Optimal technology selection and operation of commercial-building microgrids. *IEEE Trans Power Syst.* 2008;23(3):975–982. doi:10.1109/TPWRS.2008.922654.
38. Katiraei F, Iravani M. Power management strategies for a microgrid with multiple distributed generation units. *IEEE Trans Power Syst.* 2006;21(4):1821–1831. doi:10.1109/TPWRS.2006.879260.
39. Tsikalakis AG, Hatziargyriou ND. Centralized control for optimizing microgrids operation. *IEEE Trans Energy Conversion.* 2008;23(1):241–248. doi:10.1109/TEC.2007.914686.
40. Hollmuller P. Evaluation of a 5 kWp photovoltaic hydrogen production and storage installation for a residential home in Switzerland. *Int J Hydrogen Energy.* 2000;25(2):97–109. doi:10.1016/S0360-3199(99)00015-4.
41. Ulleberg O, Nakken T, Eté A. The wind/hydrogen demonstration system at Utsira in Norway: evaluation of system performance using operational data and updated hydrogen energy system modeling tools. *Int J Hydrogen Energy.* 2010;35(5):1841–1852. doi:10.1016/j.ijhydene.2009.10.077.
42. Trifkovic M, Sheikhzadeh M, Nigim K, Daoutidis P. Modeling and control of a renewable hybrid energy system with hydrogen storage. *IEEE Trans Control Syst Technol.* 2013;22(1):169–179. doi:10.1109/TCST.2013.2248156.
43. Trifkovic M, Sheikhzadeh M, Nigim K, Daoutidis P. Hierarchical control of a renewable hybrid energy system. In: *2012 IEEE 51st IEEE Conference on Decision and Control (CDC)*, Maui, HI, 2012:6376–6381. doi:10.1109/CDC.2012.6426425.
44. Ferris MC, Jain R, Dirkse S. *GDXMRW: Interfacing GAMS and MATLAB*, 2011. Available at: http://www.gams.com/dd/docs/tools/gdxmrw.pdf.

Manuscript received Nov. 23, 2013, and revision received Feb. 6, 2014.